Plasmons in vertically coupled InAs/GaAs quantum dots

Ting-Ting Kang*
Key Laboratory of Semiconductor Materials Science, Institute of Semiconductors, Chinese Academy of Sciences, P.O. Box 912, Beijing 100083, People's Republic of China

R. Q. Zhang, W. G. Hu, G. W. Cong, F. A. Zhao, X. X. Han, S. Y. Yang, X. L. Liu, Q. S. Zhu, and Z. G. Wang
Institute of Semiconductors, Chinese Academy of Sciences, P.O. Box 912, Beijing 100083, People's Republic of China
(Received 17 September 2006; revised manuscript received 16 April 2007; published 28 August 2007)

We investigate plasmon excitations in a quantum wire that consists of an infinite one-dimensional array of vertically coupled InAs/GaAs strained quantum dots (QDs). The research is carried out in the framework of random-phase approximation using effective-mass theory. Our formalism is capable of studying plasmons with strong tunneling among QDs, which frustrate the conventionally adopted tight-binding approximation. Based on this formalism, a systematic study on the intraminiband or intrasubband plasmon in vertically coupled InAs/GaAs strained QDs is presented. It is found that an increase of the dot spacing will inevitably reduce the plasmon energy. In contrast, the role of dot height is relatively complex and depends on the dot spacing. The results demonstrate the possibility to engineer collective excitations in low dimensional systems by simply changing their geometric configuration.

DOI: 10.1103/PhysRevB.76.075345 PACS number(s): 73.20.Mf, 73.21.−b, 78.67.Hc, 78.67.Lt

I. INTRODUCTION

A vertical alignment of closely stacked self-assembled quantum dots (QDs), i.e., vertically coupled QDs, was first observed in InAs/GaAs by Xie *et al.*[1] After their pioneering work, vertically coupled QDs relying on a strain-field interaction between a buried and a stacked quantum dot were also observed in many other material systems.[2] Those observations have stimulated a lot of profound research in related quantum systems, e.g., a QD molecule made of a pair of vertically stacked QDs.[3] A quantum wire composed of many vertically coupled QDs is one interesting such system.[4] Since the properties of the wire are sensitive to the tunneling between dots, it may be tuned in a manner that would be impossible with other quantum wire structures. Here, motivated by the abundant physics, we are encouraged to study collective excitations, i.e., plasmons, in this unique system.

Plasmons in two-dimensional (2D) QD arrays have been studied in the past two decades mostly in theory.[5,6] In their study, the tight-binding approximation (TBA) has usually been adopted as the theoretical foundation, which makes it possible to continue the calculation and works well in most 2D QD array systems. Even for studying plasmons in other systems with weak tunneling, TBA is still the major theoretical foundation.[7] However, this approximation requires that the tunneling be weak. In addition, too many adjustable parameters are present in TBA which affects the reliability of TBA. These traits hinder the applications of TBA in studying plasmons in systems with strong tunneling.

For one-dimensional (1D) vertically coupled strained QDs, tunneling among QDs can be controlled conveniently by simply varying the barrier thickness between the QDs. In experiments, it is easier to realize vertically coupled strained QDs if the barrier thickness is small.[8] Therefore, the assumption that tunneling is weak is not always correct in 1D vertically coupled QDs. This may be the reason why no theoretical research on plasmons in vertically coupled strained QDs has been reported even ten years after the pioneering experimental work of Xie *et al.*[1]

In this paper, in order to overcome the strong tunneling difficulty encountered by TBA, plasmons in vertically coupled strained QDs are studied with the help of effective-mass theory (EMT). Effective-mass theory has been proved to be successful in calculating the electronic structures of self-assembled QDs, including vertically coupled strained QDs.[9,10] According to EMT, guided by the Hamiltonian matrix, the wave function is expanded in a plane wave basis, and the corresponding energy is also strictly determined at the same time. In this way, the effect of finite band offset, the different effective masses of electrons, and geometrical configuration can all be reflected in the Hamiltonian matrix and taken into account. The computation burden of EMT is dependent on the number of adopted plane waves, which implies that a more isolated wave function requires more computation time. Therefore, this method is suitable in studying systems with strong tunneling, which are beyond the reach of TBA. Using EMT, the influences of geometrical configuration on plasmons, which have not been studied before, can be naturally determined. In this work, the influence of dot size and spacing on plasmon energy is emphasized.

II. THEORETICAL MODEL

To familiarize the reader with the essentials of our approach, we briefly introduce our overall strategy here. EMT and the random-phase approximation (RPA) are the two theoretical foundations of our approach. In EMT, electron-electron interactions are ignored and the single-particle picture is used to calculate the wave function and energy. In RPA, the Coulomb interaction is treated classically and exchange-correlation effects are neglected. These treatments will be highlighted throughout this paper.

Within these two frameworks, we first establish the single-particle Hamiltonian matrix considering a quantum wire structure. From this Hamiltonian matrix, the band structure and wave function of the quantum wire will be calcu-

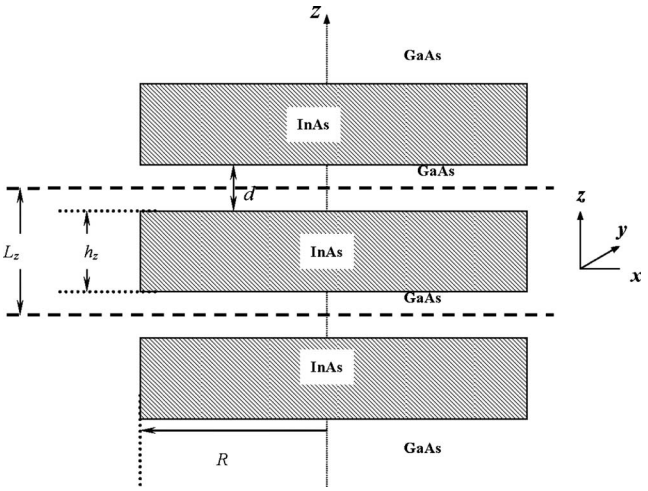

FIG. 1. Schematic of a quantum wire consisting of stacked InAs quantum dots embedded in GaAs. We choose the dashed line region as the unit cell in the z direction.

lated. Then the RPA-based generalized dielectric function $\epsilon(q,\omega)$ will be introduced with the previously obtained results from EMT, and the plasmon energies are determined by the poles of $\epsilon(q,\omega)$. We confine the numerical calculations to the case of intraminiband or intrasubband plasmons under the zero-temperature limit. Accordingly, the electron density is adjusted so that only the lowest or first subband and miniband are occupied.

The structure of a single quantum wire consisting of stacked InAs quantum dots embedded in GaAs considered here is depicted in Fig. 1. The growth direction (100) is defined as the z direction. The shape of one InAs QD is like a columnar disk, which is a rectangle in the x-z plane. In the z direction, the height of the InAs dot is h_z, and the distance between two adjacent dots is d. The period is L_z, and the radius of the dots is R. The electron potential is a constant value, namely, the InAs/GaAs conduction-band offset (V) in the GaAs and zero in the InAs QDs.

We choose the boxed region shown in Fig. 1 as the unit cell. It should be noted that the SI units, instead of Gauss units, will be used throughout this paper. In order to avoid confusion, the cited formulas will also be presented in SI units, e.g., Eq. (11).

In this system, the electron wave function can be written approximately as the product of a z dependent and an xy-dependent term:

$$\psi_{\alpha,k_z;s}(\mathbf{r}) = \varphi_{\alpha,k_z}(z)\phi_s(x,y), \tag{1}$$

where $\mathbf{r} \equiv \{x,y,z\}$. The corresponding electron energy is

$$E_{\alpha,k_z;s} = E_s + E_{\alpha,k_z}, \tag{2}$$

where α is the index of the miniband and s is the subband index. E_s arises from confinement in the x-y plane and E_{α,k_z} results from modulation in the z direction.

Considering the periodicity in the z direction, $\varphi_{\alpha,k_z}(z)$ will be calculated by EMT. According to EMT,[9,10] $\varphi_{\alpha,k_z}(z)$ can be expressed as

$$\varphi_{\alpha,k_z}(z) = \frac{1}{\sqrt{L}}\sum_{n_z} C_{\alpha,k_z,n_z} e^{i(k_z+n_zK_z)z}, \quad n_z = 0, \pm 1, \pm 2, \ldots, \quad K_z = \frac{2\pi}{L_z}. \tag{3}$$

L is the length of this quantum wire in the z direction and can be regarded as infinity. E_{α,k_z} and C_{α,k_z,n_z} are the eigenvalue and eigenvector of the Hamiltonian matrix $H(k_z)$, respectively. In the calculation, the ground miniband (or subband) is labeled as α (or s) =1. E_{1,k_z} is the smallest eigenvalue of $H(k_z)$ and C_{1,k_z,n_z} is its corresponding eigenvector. The Hamiltonian matrix of the system in Fig. 1 is placed in the Appendix. As usual, the electron-electron interactions are not included in the Hamiltonian matrix. This exclusion is also consistent with the spirit of RPA we adopt.

Within the framework of RPA,[11] following Ref. 7, we obtain the generalized dielectric function given by

$$\varepsilon_{s,s',t,t'} = \delta_{s,t}\delta_{s',t'} - \sum_{\alpha',\alpha}\sum_{n_1,n_2,n_3,n_4}\frac{1}{2\pi} \times \int dk_z C^*_{\alpha,k_z,n_1} C_{\alpha',k_z+q,n_2} C^*_{\alpha',k_z+q,n_3} C_{\alpha,k_z,n_4} \Lambda_{\alpha',k'_z=k_z+q;s';\alpha,k_z;s} F_{t,t',s,s'}[q+K_z(n_2-n_1)]\delta_{(n_2-n_1),(n_3-n_4)} \tag{4}$$

and

$$F_{t,t',s,s'}[q+K_z(n_2-n_1)] = \int d\mathbf{x}\int d\mathbf{x}'\frac{e^2}{2\pi\varepsilon_s} \times \phi^*_t(\mathbf{x})\phi_{t'}(\mathbf{x})\mathbf{K}_0\{[q+K_z(n_2-n_1)] \times |\mathbf{x}-\mathbf{x}'|\}\phi_s(\mathbf{x}')\phi^*_{s'}(\mathbf{x}'), \tag{5}$$

$$\Lambda_{\alpha',k'_z;s';\alpha,k_z;s} = 2\left[\frac{f_0(E_{\alpha',k'_z;s'}) - f_0(E_{\alpha,k_z;s})}{E_{\alpha',k'_z;s'} - E_{\alpha,k_z;s} + \hbar\omega + i\gamma}\right], \tag{6}$$

where $\mathbf{x} \equiv \{x,y\}$, δ is the usual Kronecker delta, which is unity if $(n_2-n_1)=(n_3-n_4)$ and zero otherwise, $\mathbf{K}_0(\mathbf{x})$ is the zeroth-order modified Bessel function of the second kind, γ is the damping factor, and f_0 is the Fermi distribution function. In Eq. (6), a prefactor of 2 is added to account for the spin degeneracy in the system.

Equation (4) gives the dynamic dielectric matrix, which considers both the subband induced by confinement in the x-y plane and the miniband resulting from modulation in the z direction. The plasmon spectrum is obtained by the condition when the determinant of the dielectric matrix vanishes:

$$|\varepsilon_{s,s',t,t'}(q,\omega)| = 0. \tag{7}$$

Here, we limit ourselves to the study of intraminiband and intrasubband plasmons under the zero-temperature limit. In

this case, only the lowest or first subband and miniband are occupied, while any excited subband and miniband will be ignored in the calculations. Then the dynamic dielectric function can be simplified into the following form:

$$\varepsilon(q,\omega) = \varepsilon_{1,1,1,1} = 1 - \sum_{n_1,n_2,n_3,n_4} \int dk_z C^*_{1,k_z,n_1} C_{1,k_z+q,n_2} C^*_{1,k_z+q,n_3} C_{1,k_z,n_4} \Lambda_{(1),k'_z=k_z+q;1;(1),k_z;1} F_{1,1,1,1}[q + K_z(n_2 - n_1)] \delta_{(n_2-n_1),(n_3-n_4)}. \quad (8)$$

When it is possible to confuse the index of the miniband with that of the subband, the miniband index will be placed in brackets.

For $F_{1,1,1,1}[q+K_z(n_2-n_1)]$, in the long wavelength limit, we take the approximation as in Ref. 12:

$$F_{1,1,1,1}[q + K_z(n_2 - n_1)] = \frac{e^2}{2\pi\varepsilon_s} \mathbf{K}_0\{[q + K_z(n_2 - n_1)]R\}, \quad (9)$$

where the radius of the QD(R) is taken as the characteristic cutoff length.

The single-particle excitation (SPE) region, where the plasmon is subject to Landau damping, is determined by calculating the poles of the corresponding irreducible response function,[13] i.e., the region where Eq. (10) is satisfied:

$$f_0(E_{\alpha',k_z+q;n'}) - f_0(E_{\alpha,k_z;n}) \neq 0,$$

$$E_{\alpha',k_z+q;n'} - E_{\alpha,k_z;n} = \hbar\omega. \quad (10)$$

III. NUMERICAL RESULTS AND DISCUSSION

Following the treatment in Ref. 14, we use the electron effective mass of bulk InAs under the average hydrostatic strain present in the dot material, which is calculated to be $0.04m_e$ (m_e is the free electron mass) in the conduction band. The electron effective mass in GaAs is set to $0.067m_e$. The conduction-band offset V is taken from Ref. 10 as 0.5134 eV, and the dielectric constant of GaAs is used as ε_s, i.e., $\varepsilon_s = 12.8\varepsilon_0$, where ε_0 ($\varepsilon_0 = 8.85 \times 10^{-12}$ F/m) is the dielectric constant in vacuum. For all of the following calculations, the damping factor γ is assumed to be 0.005 meV, the QD radius R is 7.5 nm, and the linear charge density takes the value of $N_L = (2/3) \times 10^6$ cm^{-1}, i.e., $k_F = (\pi/3) \times 10^6$ cm^{-1}. The numbers of plane waves used in our calculations are $n_z = 0, \pm1, \pm2, \pm3, \pm4$. Taking more plane waves, the calculated results will be slightly improved.

The evolution of the dielectric function (ε) with respect to energy is presented in Fig. 2. In the calculations, we choose $h_z = 3$ nm, $L_z = 4$ nm, and $q = (\pi/5) \times 10^5$ cm^{-1}. It is shown that when the energy approaches the SPE region, Re(ε) (the real part of ε) will rise markedly, while in the SPE region, Re(ε) experiences a drastic falling, from a large positive value to a large negative value. Since this SPE corresponds

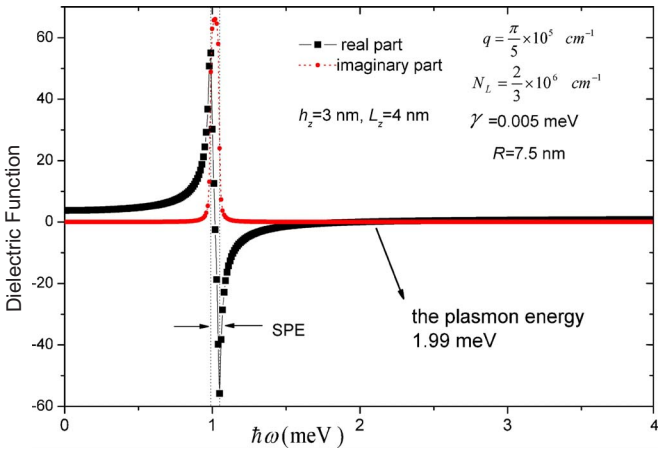

FIG. 2. (Color online) Dielectric function (ε) as a function of the energy. The calculated SPE region is indicated by dotted lines.

to intrasubband or intraminiband absorption, namely, the excitation of electron-hole pairs around the Fermi level, this behavior of Re(ε) in SPE is in agreement with that described in textbooks related to the evolution of Re(ε) in the absorption energy region. After passing SPE, a rise in Re(ε) is restored. During this transition, the plasmon energy can be determined at the point where Re(ε)=0, and we will calculate the plasmon energy (E_P) in this way. If the energy increases further, Re(ε) will be close enough to the constant value of 1, i.e., Re(ε)$\rightarrow$1. Im(ε) (the imaginary part of ε) only has a pronounced value in the SPE region, indicating strong intrasubband or intraminiband absorption in the SPE region. In other regions, due to the weak absorption described by γ, it will take a small and almost constant value. Two steps separate the terracelike SPE region from the other region. As a whole, the calculations reproduce the well-known behavior of the dielectric function, both in the real and imaginary parts.

Figure 3 depicts the plasmon energy dispersion and SPE region calculated with the same set of parameters used in Fig. 2. An additional curve, calculated according to Ref. 15,

$$E_P = \hbar q \sqrt{|\mathrm{In}(qR)|} \left(\frac{N_L e^2}{2\pi\varepsilon_s m^*} \right)^{1/2}, \quad (11)$$

is added for comparison. Equation (11) is the well-known dispersion relation for plasmon in a 1D quantum wire in the long wavelength limit.[15] Since intraminiband or intrasubband plasmons is associated with the electrons around the Fermi level, the effective mass (m^*) at the Fermi level is adopted as m^* in Eq. (11). In Eq. (11), it is assumed that m^* will not change over the entire miniband, while in our method, the variation of the effective mass around the Fermi level (m^*_F) is considered. The difference between our results and Eq. (11) means that when studying E_P in quantity, as we will do below, it may be unsafe to derive E_P simply through Eq. (11). In Fig. 4, we have calculated three dispersion curves with the same dot height but different dot spacings. It is found that the dispersion curve shifts to low energy if the QD spacing increases, i.e., under the same q, the plasmon energy is re-

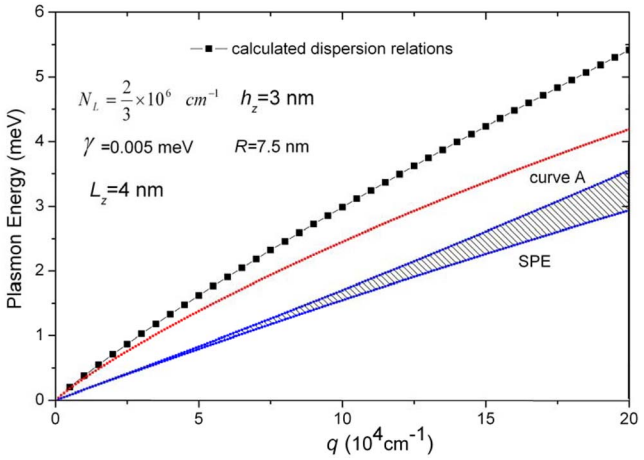

FIG. 3. (Color online) Plasmon energy dispersion and SPE region calculated with the same set of parameters used in Fig. 2. The shaded area indicates the SPE region. For comparison, curve A is presented and calculated according to Eq. (11) with $m^*=0.049\,413m_e$, which is the calculated effective mass at the Fermi level in this system.

duced. This trend can be seen more clearly in Fig. 5.

In Fig. 5, with an increase of dot spacing, E_P in all cases decreases monotonically, irrespective of dot height. This evolution indicates that reducing tunneling will result in a decrease in E_P. The effect of dot height (h_z) on E_P is complex. When $d=0$, a single InAs quantum wire is achieved, and the E_P in all cases take the same value. With a small dot spacing ($d\leqslant 1.5$ nm), where strong tunneling occurs, larger height will lead to higher plasmon energy, and the relation is reversed if the tunneling probability is reduced further ($d\geqslant 2$ nm). These results show that the roles played by dot height in determining E_P are dependent on the dot spacing. This behavior related to h_z can also be explained based on tunneling. When the QDs are well separated, the ground state in thin QDs is higher in energy, which leads to stronger tunneling and also larger E_P than thick QDs. If d is small

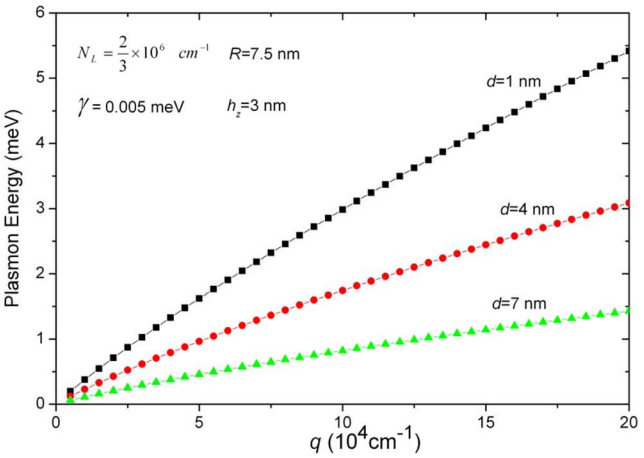

FIG. 4. (Color online) Influence of dot spacing on the dispersion relations of plasmons.

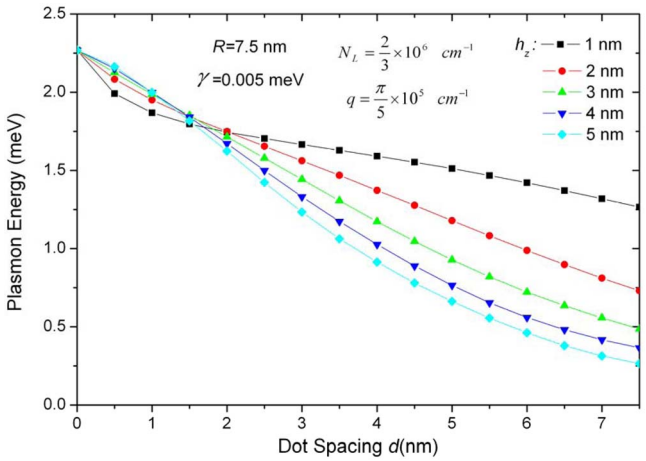

FIG. 5. (Color online) Influence of dot height and spacing on the plasmon energy.

enough, tunneling in thin QDs will face not only the nearby barriers but also the successive barriers, resulting in low tunneling. Considering the positive influences exerted by tunneling on E_P, all of the relations described above are well explained.

In the view of TBA, the energy of an adopted Wannier wave function centered at a QD will decrease as the QD becomes thicker. As a result, with the same dot spacing, the tunneling between thick QDs will be reduced, leading to the reduction of E_P. However, these predictions can only explain the results related to E_P and h_z in Fig. 5 when $d\geqslant 2$ nm. When $d\leqslant 1.5$ nm, thicker QDs will have larger E_P and these predictions break down. The failure of TBA is not surprising given the fact that only tunneling from the nearest QDs is included in TBA.

We know that the miniband structure can be parametrized by the effective mass. On the other hand, the similarity between the fitting curves, which rely on m^* at the Fermi level (m_F^*), and the calculated curve is shown in Fig. 3. Therefore, it may be instructive to investigate the evolution of the ef-

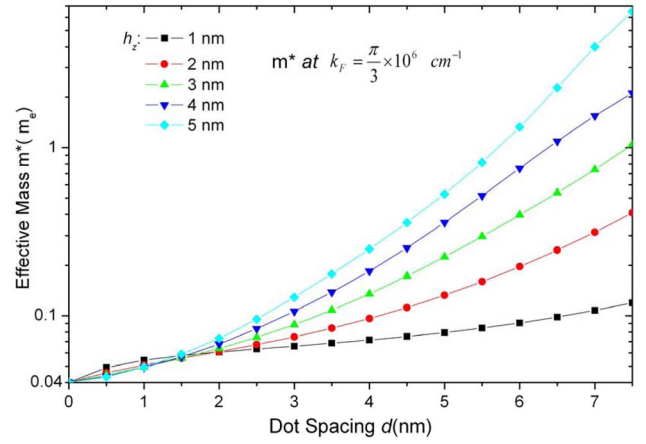

FIG. 6. (Color online) Evolution of the effective mass at the Fermi level (m_F^*) with respect to dot height and spacing. The effective mass is in the unit of the free electron mass.

fective mass. The calculated results for m_F^* are presented in Fig. 6. When $d=0$, i.e., the situation of an InAs quantum wire, effective masses of all cases converge to $0.04m_e$, the adopted electron effective mass in strained InAs QDs. With increasing dot spacing, the effective mass increases quickly, reflecting the exponentially suppressed tunneling probability. This trend is in agreement with the previous calculations'.[4] The turning point, where the effect of dot height on E_P is reversed, also appears at $d=1.5$ nm in Fig. 6. Since E_P shows a $1/\sqrt{m^*}$ dependence, as shown in Eq. (11), the evolution of m_F^* can be used to explain completely the situations in Fig. 5. These correlations show in our system that m_F^* is a representative parameter in evaluating the overall miniband states that participate in intraminiband or intrasubband plasmons, or, simply speaking, a small value of m_F^* means that other miniband states around the Fermi level that participate in intraminiband or intrasubband plasmons will also have small m^*. For other plasmon modes, such as interminiband or intersubband plasmons, the situation is more complex. This is because not only the states around the Fermi level but also the whole ground miniband or subband will contribute to the collective excitations. A single parameter like m_F^* may be insufficient to account for those complexities.

At the end of this section, we give a brief discussion of the limits of applicability of our method. It seems that our method is a precise approach which can be applied to systems with weak tunneling. However, if the tunneling is too weak, intradot electron-electron interactions will be prominent and must be considered when determining the band structure. Unfortunately, we cannot consider those interactions with the single-particle EMT method. On the other hand, with the reduction of tunneling, the electron will be very localized, requiring a greater number of plane waves and increasing the calculation burden in EMT to an unmanageable level. Therefore, the applicability of our method should be limited to the range from strong tunneling to medium tunneling. In this range, tunneling integral is greater than intradot Coulomb interaction and the calculation burden is manageable.

IV. CONCLUSION

In summary, the plasmon excitation in one quantum wire consisting of an infinite 1D array of vertically coupled InAs/GaAs quantum dots has been studied based on effective-mass theory and the random-phase approximation. This study covers the calculation of the dielectric function, the dispersion relations, and the influence of geometric configuration on plasmon energy. It is found that the enhancement of tunneling among QDs will increase the plasmon energy. The study also provides some guidelines for engineering the collective excitations in vertically coupled quantum dots.

ACKNOWLEDGMENTS

This work was supported by the Special Funds for Major State Basic Research Project (No. G20000683) and National Science Foundation of China (No. 60376013, No. 60506002, and No. 60136020).

APPENDIX: HAMILTONIAN MATRIX

According to effective-mass theory and taking into account the differences of the effective masses between InAs and GaAs materials, the electron Hamiltonian can be written as the equation below (neglecting the second- and higher-order terms in the approximation):

$$H_e = \mathrm{P}\frac{1}{2m^*(\mathbf{r})}\mathrm{P} + V_e(\mathbf{r}). \tag{A1}$$

In the unit cell in Fig. 1, the matrix elements of the Hamiltonian can be written as

$$\left(\frac{\hbar^2 k_{n,n'}^2}{2m_{\mathrm{GaAs}}^*} + V\right)[\delta_{n,n'} - S(h_z)] + \frac{\hbar^2 k_{n,n'}^2}{2m_{\mathrm{InAs}}^*} S(h_z), \tag{A2}$$

$$S(h_z) = \begin{cases} \dfrac{\sin\left[\dfrac{\pi h_z (n-n')}{L_z}\right]}{\pi(n-n')} & \text{for } n \neq n' \\ \dfrac{h_z}{L_z} & \text{for } n = n', \end{cases} \tag{A3}$$

$$k_{n,n'} = \sqrt{(k_z + nK_z)(k_z + n'K_z)}. \tag{A4}$$

*Author to whom correspondence should be addressed; ktt219@163.com

[1] Qianghua Xie, Anupam Madhukar, Ping Chen, and Nobuhiko P. Kobayashi, Phys. Rev. Lett. **75**, 2542 (1995).
[2] J. Stangl, V. Holý, and G. Bauer, Rev. Mod. Phys. **76**, 725 (2004).
[3] T. Ota, M. Rontani, S. Tarucha, Y. Nakata, H. Z. Song, T. Miyazawa, T. Usuki, M. Takatsu, and N. Yokoyama, Phys. Rev. Lett. **95**, 236801 (2005).
[4] Craig Pryor, Phys. Rev. Lett. **80**, 3579 (1998).
[5] Nammee Kim and Sergio E. Ulloa, Phys. Rev. B **48**, 11987 (1993); Danhong Huang and P. R. Antoniewicz, *ibid.* **43**, 2169 (1991).
[6] Weiming Que, Phys. Rev. B **47**, 1636 (1993); Weiming Que, George Kirczenow, and Eleuterio Castano, *ibid.* **43**, 14079 (1991); Wei-ming Que and George Kirczenow, *ibid.* **38**, 3614 (1988).
[7] M. S. Kushwaha and H. Sakaki, Phys. Rev. B **69**, 155331 (2004).
[8] M. Meixner and E. Schöll, Phys. Rev. B **67**, 121202(R) (2003).
[9] Shu-Shen Li, Kai Chang, and Jian-Bai Xia, Phys. Rev. B **71**, 155301 (2005).
[10] S.-S. Li, J.-B. Xia, Z. L. Yuan, Z. Y. Xu, W. Ge, X. R. Wang, Y.

Wang, J. Wang, and L. L. Chang, Phys. Rev. B **54**, 11575 (1996).
[11] H. Ehrenreich and M. H. Cohen, Phys. Rev. **115**, 786 (1959).
[12] S. Das Sarma and W. Y. Lai, Phys. Rev. B **32**, 1401 (1985).
[13] S. Das Sarma and Daw-Wei Wang, Phys. Rev. Lett. **83**, 816 (1999).
[14] M. A. Cusack, P. R. Briddon, and M. Jaros, Phys. Rev. B **54**, R2300 (1996).
[15] Q. P. Li and S. Das Sarma, Phys. Rev. B **43**, 11768 (1991).